



Senseable City Lab :::: Massachusetts Institute of Technology

This paper might be a pre-copy-editing or a post-print author-produced .pdf of an article accepted for publication. For the definitive publisher-authenticated version, please refer directly to publishing house's archive system

<https://doi.org/10.1038/s42949-025-00295-9>

Unveiling the internal structures of informal settlements through AI-driven automated segmentation of LiDAR data

Check for updates

Chang Liu¹, Kee Moon Jang¹, Stefania Dimitrov^{1,2}, Cezar Lima Ferreira Barbalho³, Fabio Duarte¹ ✉ & Carlo Ratti^{1,4}

Approximately 23% of Rio de Janeiro's population, around 1.5 million people, live in *favelas*, a form of informal settlement in Brazil. These communities often lack essential infrastructure and are disproportionately impacted by environmental and public health challenges linked to their complex and irregular urban morphology. Given their scale and significance, a comprehensive understanding of the spatial configuration of these communities is critical. Yet, conventional top-down mapping methods fail to adequately capture the vertical and spatial intricacies within these environments. This research proposes a novel framework that incorporates a semantic segmentation procedure for three-dimensional (3D) scene understanding of favelas using a wearable Light Detection and Ranging (LiDAR) dataset and an artificial intelligence (AI)-driven approach. High-resolution point clouds collected in the Vidigal favela were used to train a semantic segmentation model that accurately classifies seven key object categories relevant to the 3D morphology of informal settlements, including ground, vegetation, building, wire, rock, pole, and movable objects. Our results highlight the effectiveness of point level feature engineering and multiscale neighborhood analysis for accurate segmentation of objects in dense and irregular informal environments. This approach provides a scalable way to capture the internal spatial complexity of informal settlements, supporting data-driven planning, risk assessment, and equitable infrastructure development in otherwise inaccessible areas.

According to the 2020 United Nations report, around 1.1 billion people currently live in informal settlements worldwide, and this number is expected to increase by an additional 2 billion by 2050¹. It is imperative to monitor the expansion of informal settlements for efficient urban planning aimed at overcoming the conditions of deprivation to which these territories have been historically subjected. Among the 17 United Nations Sustainable Development Goals, at least four goals mention the improvement of living conditions of the inhabitants in informal settlements, including Goal 3—good health and well-being, Goal 6—clean water and sanitation, Goal 9—industry, innovation, and infrastructure, Goal 11—sustainable cities and communities². Informal settlements, often characterized by precarious constructions, lack of basic infrastructure, informal urban planning, and densely populated settlements, exhibit complex and irregular internal structures that reflect the socioeconomic dynamics and historical evolution of these communities. Understanding these structures is crucial for addressing issues related to urban planning, resource allocation, and social equity. Several studies have discussed the environment of informal settlements,

particularly from a transportation perspective, underscoring the importance of monitoring road networks to improve access to basic infrastructure services within these informal settlement areas³. Moreover, an enhanced understanding of the internal morphology can benefit environmental planning^{4,5}, disaster risk management^{6–8}, and community development⁹ in these areas. However, the lack of adequate infrastructure in many informal settlements, including informal water and sewage networks and irregular pedestrian pathways, hinders access to basic services and internal mobility. Therefore, it is necessary to employ detection technologies to understand the inside road networks and morphology of informal settlements.

With the technological development of remote sensing and artificial intelligence (AI) methods, there has been an increasing amount of research efforts on mapping informal settlements using high-resolution satellite or aerial imagery^{10–12}. This enabled a more efficient data collection and analysis framework to detect the outer boundaries of informal settlements from above, overcoming the labor-intensive nature of traditional land surveying activities. However, most of the previous projects focused on top-down two-

¹Senseable City Lab, Massachusetts Institute of Technology, Cambridge, MA, USA. ²Universidade Presbiteriana Mackenzie, São Paulo, SP, Brazil. ³Sondotécnica Engenharia de Solos S.A., São Paulo, SP, Brazil. ⁴Dipartimento ABC, Politecnico di Milano, Milan, Italy. ✉e-mail: fduarte@mit.edu

dimensional (2D) observations, missing important parts of the internal spatial complexity of informal settlements. More recently, airborne Light Detection and Ranging (LiDAR) has been applied for informal settlement mapping by capturing the three-dimensional (3D) topography to understand the vertical structure of informal settlements^{13,14}. Yet, due to the informality of the built environment in these neighborhoods, both satellite images and airborne LiDAR do not fully reach the ground level to adequately scan the road structure or facilities. Also, the use of LiDAR point clouds was restricted to classifying ground and non-ground points, whereas object-level knowledge on the location, the structure, and morphology of informal settlements remains to be obtained^{15,16}. While computer vision and photogrammetry communities have developed deep neural networks for various point cloud segmentation tasks^{17–22} and introduced benchmark datasets for 3D scene understanding (i.e., SemanticKITTI²³, Paris-Lille-3D²⁴, Toronto-3D²⁵, Campus3d²⁶, ZAHA²⁷), they are mostly targeted at understanding street or building characteristics in an open environment, limiting their applicability in natural scenes with high complexity and density like informal settlements. Moreover, deep learning always requires large annotated training datasets and substantial computational resources, which are often difficult to obtain in the context of informal settlements.

Rio de Janeiro, Brazil, has a population of 6.2 million, with approximately 23% living in favelas, densely populated informal settlements often located along the steep hillsides and narrow roads^{28,29}. Nevertheless, as defined by the Prefeitura da Cidade do Rio de Janeiro (Rio de Janeiro City Hall)³⁰—predominantly residential building usage, low-income residents, lack of legal status (i.e., formal subdivision, ownership, compliance with construction standards), deficient urban infrastructure or public services, and informal occupation with narrow streets and irregular alignment—undesirable living conditions still persist jeopardizing the quality of life of inhabitants in favelas. Dwellings built on uneven terrain, such as hillsides, can lead to poor drainage and increased vulnerability to landslides. The spatial proximity between affluent and low-income areas in coastal zones reflects the sharp contrasts in access to infrastructure and services. An earlier study conducted a morphometric analysis on terrestrial LiDAR data by extracting planar geometries from street scenes of Rocinha, the largest favela in Rio de Janeiro³¹. However, a plane extraction model could not provide any understanding of scene elements, and the analysis was made for only two areas in Rocinha. Moreover, compared with traditional terrestrial laser scanning, wearable LiDAR offers greater flexibility and efficiency in geometrically complex environments, such as the narrow alleyways of informal settlements, making it a suitable choice for this research³². Therefore, a scalable data collection and analysis framework with a more convenient device, such as a wearable LiDAR, is necessary to unveil the internal spatial complexity of favelas, assisting data-driven urban planning and management of informal settlements.

Given that the structure and morphology of the informal settlements vary by location, even within a single community¹¹, this research aims to propose a generalizable AI-driven framework that incorporates a semantic segmentation procedure enabling a 3D favela scene understanding at eye level.

The procedure contains three steps, including data collection and labeling, training a machine learning model, and testing and evaluating the performance and feature importance of the model. First, a wearable LiDAR scanning device was used to collect point clouds of the Vidigal favela in Rio de Janeiro, from which a subset was manually labeled for seven classes that represent scene elements in favelas. The observed morphological patterns, such as vertical layering, variations in density, and structural complexity, motivate the labeling of these seven specific object classes to capture their distinctive characteristics. Then, we applied a machine learning-based model to segment points into one of the seven classes. After that, the importance of neighborhood features at different scales was computed to identify what factors were more contributive in classifying objects in the favela environment.

This research introduces a novel methodological approach for learning the semantics of internal scenes of informal settlements from point clouds

collected using a wearable LiDAR device, addressing the limitations of conventional top-down mapping methods. From an applied perspective, this research generates detailed, data-driven insights into the unique morphology of informal settlements and supplements incomplete spatial information, thereby supporting risk assessment, equitable infrastructure development, and evidence-based urban planning and policy.

Results

Semantic segmentation of favelas with machine learning

In order to learn the semantics of object categories existing in the informal settlements, a manually labeled point cloud is needed. Considering the data processing capability of the computer, the original collected Vidigal dataset was cleaned and subsampled to contain 625 K points. Then, we manually annotated this subset with seven different labels that typify the physical environment of favelas: ground, vegetation, building, movable, wire, rock, and pole. “ground” and “building” are the basic elements in favelas. “vegetation” and “rock” represent natural elements, whereas “wire” and “pole” are labeled for man-made elements that are frequently found in favelas. Note that the “movable” category refers to temporary elements such as a person, vehicle, or motorcycle. These non-permanent elements are not the primary focus of this research and were grouped into a single “movable” category to simplify the classification scheme and reduce model complexity. As the ultimate goal of having a detailed 3D model is to inform physical interventions in informal settlements to improve their living conditions, movable objects are not considered here. In addition, these object types represent only a small fraction of the total points in our dataset. If treated as separate classes, the already limited number of points for each would become even smaller, potentially leading to unstable model training and unreliable evaluation metrics. Therefore, this is added to the six physical object features identified from the previous section to distinguish any non-permanent object during scanning. The labeling process includes separating the ground from non-ground points using the cloth simulation filter³³ and segmenting the non-ground into each of the other six classes with visual interpretation. The labeled dataset was split into 80% *TrainSet* (500 K points) and 20% *TestSet* (125 K points), which are mutually exclusive to avoid any spatial bias or accidental overlaps. 20% points of *TrainSet* were applied for validation.

Fig. 1a displays the color information, and Fig. 1b shows the unstructured raw point clouds. Fig. 1c presents the labeled *TrainSet*, and Table 1 provides an overview of the seven classes along with their respective number of points. “Building” accounts for nearly 60% of the points in the training data, exhibiting a highly dense environment of informal settlements.

In this research, a random forest-based 3D Multi-Attributes, Multi-Scale, Multi-Cloud (3DMASC) model³⁴ was adopted for the classification of favelas’ built environments captured using wearable LiDAR. 3DMASC incorporates both point and neighborhood features to predict class labels of unstructured point clouds with proven suitability in natural or semi-urban contexts, and can be performed in an accessible and efficient manner through an open-source plugin within the CloudCompare software. Table 2 provides the complete list of features used for the 3DMASC implementation, which includes 4 point features and 20 neighborhood features using a spherical neighborhood. Point features in the table include three color bands: red (R), green (G), and blue (B), and point intensity. Point intensity in LiDAR is “the return strength of the laser pulse that generated the point”³⁵. Moreover, this research computed descriptive features in several neighborhoods of different scales. Neighborhood features were calculated at scales of 0.25 (SC0.25), 1 (SC1), and 5 (SC5) meters radii, considering the narrow width (2–3 m) of alleys in Vidigal. Moreover, these three scales were designed to capture spatial characteristics at fine, intermediate, and broad neighborhood scales, respectively. The 0.25 m scale enables the extraction of fine-grained details and surface noise, which is especially useful for detecting small or sharply defined structures, such as poles. The 1 m scale provides micro-topographic features and subtle surface variations, making it effective for identifying slope transitions and small-scale objects, such as rocks and

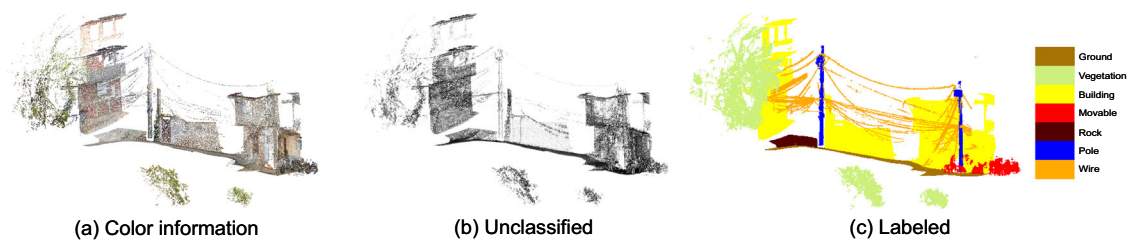


Fig. 1 | Three formats of *TrainSet* point clouds. This is a sample of *TrainSet*. The *TrainSet* was used for training and validating the 3DMASC model to segment LiDAR point clouds into seven classes. **a** Color information of the sample data. **b** Unclassified raw uncolonized sample data. **c** Seven labeled classes in sample data. Golden brown: Ground; Light green: Vegetation; Yellow: Building; Red: Movable; Orange: Wire; Maroon: Rock; Blue: Pole.

Table 1 | Number of points for each class in *TrainSet*

Class no.	Label	No. of points
1	Ground	70,415
2	Vegetation	51,667
3	Building	298,321
4	Movable	18,140
5	Wire	24,646
6	Rock	20,842
7	Pole	15,969
	Total	500,000

low-rise buildings. The 5 m scale is suitable for capturing a broader context, such as buildings and vegetation. The random forest parameters were set as “max depth” 40, “max tree count” 150, “active var count” 0, and “min sample count” 20. Those 24 features were chosen because they can reflect different types of information of point clouds and have been applied in previous studies^{36,37}. The 20 neighborhood features were separated into three categories: statistics-based, dimensionality-based, and geometry-based. Those nine statistics-based features inform the echo information of the point cloud. It should be noted that the dimensionality-based features are essentially a subset of geometry-based features, explicitly focusing on the spatial dimensional distribution characteristics. Those dimensionality-based features describe the general aspect of the local point cloud and identify if the target has a spherical, linear, or planar structure. The terms l_1 , l_2 , and l_3 in Table 2 refer to the three eigenvalues derived from the covariance matrix of points within a local neighborhood obtained through Principal Component Analysis (PCA)³⁶. They are sorted in descending order. Geometry-based neighborhood features reflect the shape of the point cloud. The performance of the trained classifier was evaluated with metrics, including the overall accuracy of the model as well as precision, recall, and F1-score for each class label. Feature importance is also presented as Shapley values³⁸ for the explainability of prediction results.

Three metrics, including precision, recall, and F1-score, were adopted as evaluation metrics. The precision represents how many points are detected correctly of all the points the model labels as positive, as stated in Eq. 1. Recall, as shown in Eq. 2, reflects the percentage of the positive points detected successfully among all the actual positive points (TP and FN). The F1-score shown in Eq. 3 is the harmonic mean of precision and recall. F1-score gives equal importance to both precision and recall, a single number that balances the trade-off between precision and recall.

$$Precision = \frac{TP}{TP + FP} \tag{1}$$

$$Recall = \frac{TP}{TP + FN} \tag{2}$$

$$F1 = 2 \times \frac{Precision \times Recall}{Precision + Recall} \tag{3}$$

where *TP*, *FN*, and *FP* are true positive, false negative, and false positive by point, respectively.

Model performance

Similar to Figs. 1 and 2 presents the details of the *TestSet*, including the RGB color information (Fig. 2a), the unstructured raw point clouds (Fig. 2b), and the test result with seven classes (Fig. 2c). As a result, as shown in Fig. 3a, the trained 3DMASC classifier demonstrated an accurate prediction of favelas class labels in the *TestSet* with an overall accuracy of 94.55%. The TP proportion of each class is 13.12%, 10.39%, 56.72%, 3.64%, 4.85%, 3.92%, and 1.91%. The total sum of these values is 94.55%, which is the overall accuracy.

Meanwhile, the performance of each label varies, as indicated by the evaluation metrics in Fig. 3b. For instance, “ground” and “building” were successfully predicted with high precision (91.12% and 93.54%, respectively) and recall (97.34% and 95.09%, respectively), which indicates the model’s capability to precisely delineate the built environment of favelas. The relatively high performance of these two classes was likely attributed to their larger number of points in the training set, which reflects the effect of class imbalance on model performance. The few errors that occurred involved misclassifications between these two classes or incorrect assignments to the ‘vegetation’ class. This is reasonable as distinguishing between ground and building at ground level or building and vegetation at higher vertical positions from the scanned point clouds can be challenging, even through visual inspection, due to the hilly topography. Segmented building and ground points from unstructured point clouds can serve as a basis for illustrating the arrangement of buildings and thus improving the coverage of spatial information at the ground level that could not be observed via airborne photography or LiDAR. A particularly unanticipated result was that almost all “vegetation” points were categorized correctly. This shows that the classifier achieved perfect recall and was successful in understanding the irregular geometries and unique shapes of green elements along the narrow alleys of the Vidigal favela. However, its precision was the lowest (84.62%) as several points were predicted as “vegetation” wrongly (mostly the “building” class). Labels such as “movable,” “wire,” and “rock” showed a balanced prediction with F1-scores over 90%. Notably, the “movable” points were classified with high precision and recall, demonstrating that non-permanent objects (such as people, vehicles, and motorcycles) can be effectively filtered from the scanned point clouds to create a clear 3D representation of the built environment in the favela. In contrast, 40% of real “pole” points were misclassified as other vertical elements, despite high precision in their prediction.

Feature importance

As an explainable approach, we further identified the contributions of each feature to the prediction of favela class labels. Fig. 4 shows the mean absolute Shapley value of each feature, which indicates the feature importance for the 3DMASC classification³⁴. The Shapley value comes from cooperative game theory and is widely utilized in machine learning to measure feature

Table 2 | Summary of features used for 3DMASC classification

Category	Feature	Definition	Scale
Point features	R	Red channel	0
	G	Green channel	
	B	Blue channel	
	INT	Laser reflected intensity	
Statistics-based neighborhood features	INT_MEAN	Laser reflected intensity (mean)	0.25; 1; 5 (m)
	INT_MEDIAN	Laser reflected intensity (median)	
	INT_MODE	Laser reflected intensity (mode)	
	INT_STD	Laser reflected intensity (standard deviation)	
	INT_SKEW	Laser reflected intensity (skewness)	
	Dip	Dip angle	
	Z_STD	Elevation (standard deviation)	
Dimensionality-based neighborhood features	Z_SKEW	Elevation (skewness)	
	Zmin	Core point elevation minus the minimum elevation in the spherical neighborhood	
	PCA1	PCA: $l_1/(l_1 + l_2 + l_3)$	
	PCA2	PCA: $l_2/(l_1 + l_2 + l_3)$	
	PCA3	PCA: $l_3/(l_1 + l_2 + l_3)$	
	SPHER	Sphericity: l_3/l_1	
Geometry-based neighborhood features	LINEA	Linearity: $(l_1 - l_2)/l_1$	
	PLANA	Planarity: $(l_2 - l_3)/l_1$	
	ROUGH	Roughness	
Geometry-based neighborhood features	CURV	Mean of principal curvatures	
	NBPTS	Number of points at given scale	
	ANISO	Anisotropy: Ratio of distance to center of mass and radius of sphere	
	FOM	First order moment ⁵³	

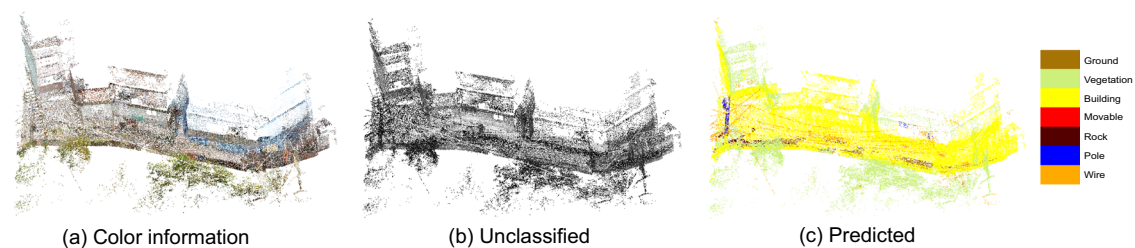


Fig. 2 | Three formats of TestSet point clouds. This is a sample of TestSet. The TestSet was used for testing the trained 3DMASC model to segment LiDAR point clouds into seven classes. **a** Color information of the sample data. **b** Unclassified raw

uncolonized sample data. **c** Predicted results of the seven labeled classes in the sample data. Golden brown: Ground; Light green: Vegetation; Yellow: Building; Red: Movable; Orange: Wire; Maroon: Rock; Blue: Pole.

contributions³⁸. These values fall within the range of 0–1, where a higher value indicates a stronger influence of the corresponding feature on the predictions.

Overall, neighborhood features were found to be more informative than point features, where dip angle (Dip_SCx), intensity (INT_SCx), elevation (Z_SCx), and number of points (NBPTS_SCx) were among the highest importance group as opposed to color channels (R, G, B) or point-level intensity (INT_SC0) observed at the lower tail. Shapley values of the four-point features were lower than 0.002, suggesting that removing them may not significantly affect the model’s decisions. Although RGB colors, along with laser intensity values, have been considered valuable semantic information for segmenting point clouds based on their appearance or texture^{39–41}, our results suggest that features computed for neighborhoods of each point may contribute more significantly to point cloud classification in a uniquely complex and dense environment of favelas. Particularly, a scale of 5 m to define spherical neighborhoods was with the highest mean importance, whose average value is nearly three times SC0.25 and two times SC1

average values. It corroborates a previous finding of an optimal scale range at small to medium diameters smaller than 7 m³⁴. This increasing trend in Shapley values suggests that broader neighborhood sizes offer more discriminative and stable feature representations. At finer scales, the extracted features may be overly sensitive to noise or local variations, limiting their utility for classification. In contrast, larger neighborhoods capture more holistic geometric patterns and context information, thereby enhancing the importance of certain features in the model’s decision-making process. Yet, the contribution of other dimensionality- or geometry-based features (i.e., sphericity, linearity, planarity, curvature, roughness) was marginal, implying that the distinct landscape structure outweighs the importance of object-level geometries for their classification.

As Table 1 mentioned, neighborhood features were categorized according to three feature categories and three scales. Fig. 5 illustrates the importance of neighborhood features grouped into these three categories, statistics-based (left), dimensionality-based (middle), and geometry-based (right), across three spatial scales. First, for statistics-based features, their

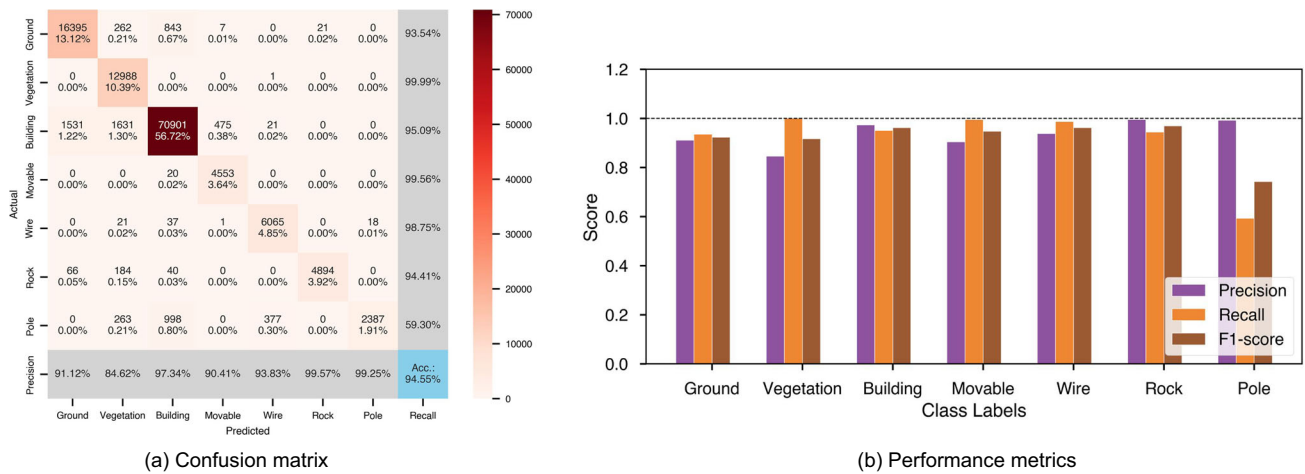


Fig. 3 | Evaluation of 3DMASC classification for TestSet. a In the confusion matrix, the bottom gray row and the right gray column indicate the precision and recall of the prediction of each class, respectively. Each red cell in the confusion matrix displays the point count and its proportion relative to the total number of points.

Dark red cells correspond to higher counts of points. For instance, 16,395 with 13.12% in the ground class means that the point number of this cell is 16,395, and 16,395 out of 125 K is 13.12%. b Three performance metrics, including Precision, Recall, and F1-score of the 3DMASC model, were calculated.

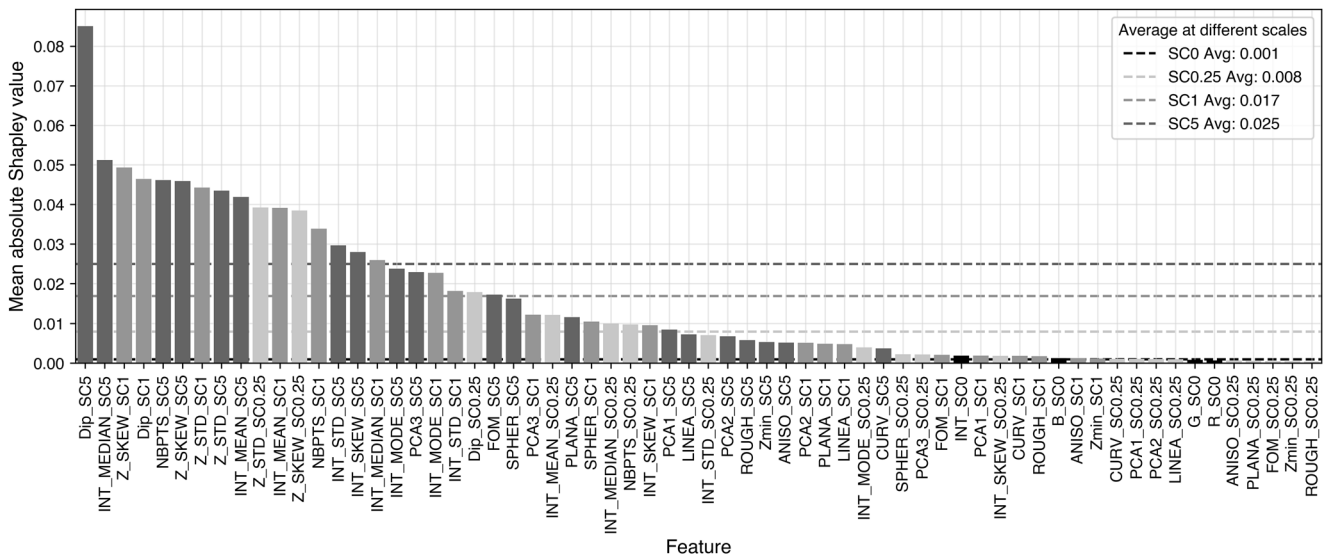


Fig. 4 | Feature importance with mean absolute Shapley values at different scales. SC0 is the scale of 0, which means there is no scale considered for point features. SC0.25, SC1, and SC5 mean that neighborhood features were calculated at scales of 0.25, 1, and 5 m radii, respectively. Black dashed line: Mean absolute Shapleys of

point features; Light gray dashed line: Mean absolute Shapleys of neighborhood features at SC0.25; Medium gray dashed line: Mean absolute Shapleys of neighborhood features at SC1; Dark gray dashed line: Mean absolute Shapleys of neighborhood features at SC5.

significance varied at different scales. For instance, elevation standard deviation (Z_STD) and elevation skewness (Z_SKEW) values were the two highest at SC0.25, whereas Z_SKEW and Dip, and Dip and INT_MEDIAN were the two most important features at SC1 and SC5, respectively. While Dip angle was found as the most dominant feature among all 64 features (see Fig. 5), indicating that surface orientation is particularly crucial in differentiation object classes in favelas from a broader scale, this may not always generalize across different spatial contexts, implying the importance of other attributes as a highly robust and discriminative feature for point cloud segmentation at various scales. Meanwhile, among elevation-related features, Z_STD and Z_SKEW showed much higher importance than Zmin at every scale, which was the simple difference between core point elevation and the local minimum. Additionally, while most statistics-based features showed their effectiveness in capturing global structural patterns by achieving the highest Shapley values at a larger scale (5 m), Z_STD and Z_SKEW showed peak importance at the intermediate scale (1 m). This

may be because these features can capture the overall variability and asymmetry of local elevation that are more robust for characterizing complex terrain at an intermediate scale. In contrast, Zmin lacks contextual depth, which may make it more sensitive to local noise or outliers.

In case of dimensionality-based neighborhood features, as shown in the middle part of Fig. 5, the two highest dimensionality-based values at all scales were PCA3 and sphericity (SPHER). Given that both features indicate the compactness of point distribution in the local neighborhood, the results show their strong discriminative power in distinguishing between planar structures (e.g., road surface, building facade) or volumetric geometries (e.g., tree canopy, rock) from the scanned favela point cloud data. The rightmost part of Fig. 5 shows geometry-based neighborhood features. Number of points (NBPTS) performed best within this category regardless of scale, indicating the critical role of local point density for the point cloud segmentation task in this research. At larger scales, this feature became increasingly reliable, plausibly due to capturing broader structural

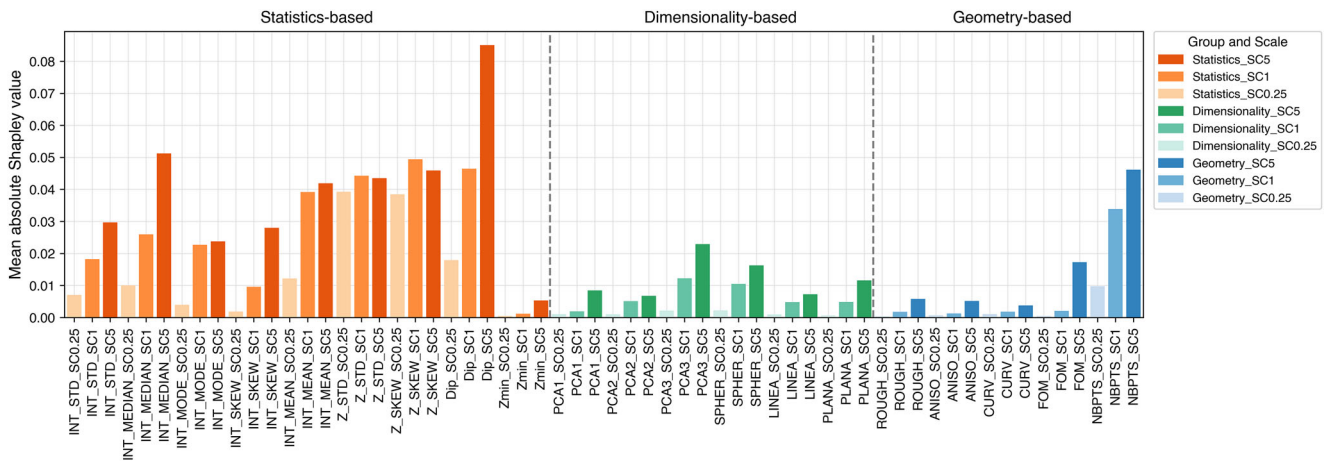
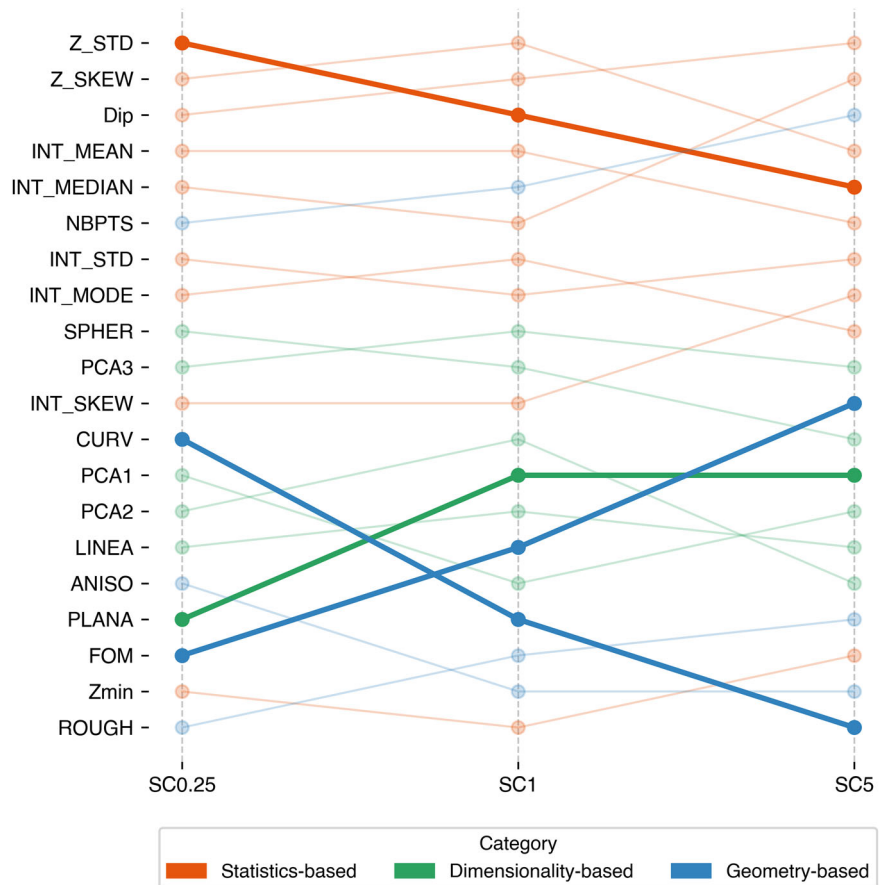


Fig. 5 | Mean absolute Shapley values of neighborhood features separated by three categories. SC0.25, SC1, and SC5 mean that neighborhood features were calculated at scales of 0.25, 1, and 5 m radii, respectively. Dark orange bar: Mean absolute Shapleys of statistics-based neighborhood features at SC5; Medium orange bar: Mean absolute Shapleys of statistics-based neighborhood features at SC1; Light orange bar: Mean absolute Shapleys of statistics-based neighborhood features at SC0.25; Dark green bar: Mean absolute Shapleys of dimensionality-based

neighborhood features at SC5; Medium green bar: Mean absolute Shapleys of dimensionality-based neighborhood features at SC1; Light green bar: Mean absolute Shapleys of dimensionality-based neighborhood features at SC0.25; Dark blue bar: Mean absolute Shapleys of geometry-based neighborhood features at SC5; Medium blue bar: Mean absolute Shapleys of geometry-based neighborhood features at SC1; Light blue bar: Mean absolute Shapleys of geometry-based neighborhood features at SC0.25.

Fig. 6 | Ranking trend of neighborhood features with the increase of the scale. SC0.25, SC1, and SC5 mean that neighborhood features were calculated at scales of 0.25, 1, and 5 m radii, respectively. Orange circle: Mean absolute Shapleys of statistics-based neighborhood features; Green circle: Mean absolute Shapleys of dimensionality-based neighborhood features; Blue circle: Mean absolute Shapleys of geometry-based neighborhood features. Four darker lines represent the four features whose ranking changed notably (more than or equal to 4) across the scale, including one statistics-based, one dimensionality-based, and two geometry-based features.



characteristics and smoothing out local variations or noise. Therefore, point count effectively encodes spatial compactness and complexity, successfully segmenting object classes that either have dense regular surfaces or sparse irregular structures. However, the values of other geometry-based features were mostly less than 0.005, which suggests that the contribution of

neighborhood geometry to the overall segmentation performance was relatively minor except NBPTS.

Fig. 6 displays the rankings of the 20 features at different scales, which reflect how feature importance changes with the scale. Generally, statistics-based neighborhood features had higher rankings than the other two

categories at each scale. However, this was not uniform across all statistics-based features, indicating internal variability in their relevance. In particular, darker lines represent the four features whose ranking changed notably (more than or equal to 4) across the scale. The first order moment (FOM) measures the center mass of a given geometry, and its steep increase indicates that the capacity to characterize asymmetric mass distribution within a neighborhood becomes more meaningful at higher scales. Similarly, Planarity (PLANA) showed an increase from 17th to 13th, implying that planar structures such as building facades and ground surfaces are more accurately represented in broader neighborhoods. Reversely, we observed decreasing patterns at larger scales. For instance, Z_STD , which was a feature of highest importance, drops to 5th (although maintaining a relatively high rank), showing that vertical variability becomes less informative in the scanned dataset at bigger scales. Meanwhile, the mean of principal curvatures (CURV) dropped from 12th to 20th, the lowest among all features. Despite the importance of CURV to delineate small-scale surface variations, its sensitivity is smoothed out at larger neighborhood sizes, reducing its ability to capture different local geometries. These shifts highlight the scale-dependent nature of neighborhood features and the importance of multi-scale feature design for object-level 3D scene understanding in the Vidigal favela.

Discussion

The complexity of defining a favela extends beyond simply mapping the spatial distribution of informal housing, making the analysis of its internal 3D morphology significantly more challenging compared to formal settlements. This research addressed this challenge by utilizing a wearable LiDAR scanning device to gather detailed spatial information with machine learning-based semantic segmentation. The case study is the Vidigal favela in Rio de Janeiro, Brazil.

The segmented object classes provide crucial socio-environmental insights to inform future urban planning strategies and support the sustainable development of favelas. Identifying ground features helps assess road conditions, including uneven, narrow, or unpaved surfaces that impede pedestrian and vehicular movement, highlighting areas needing connectivity and safety improvements. Buildings provide information on housing density, structural risks, and proximity to roads, guiding interventions aimed at improving housing conditions and mitigating risks such as fire or collapse. Vegetation distribution offers insights into environmental quality and potential resilience, suggesting opportunities for enhancing green spaces. Rocks identified within the LiDAR data signify the potential of geophysical hazards, which are critical for disaster risk mitigation planning. Infrastructure elements like electrical poles and wires reveal the condition and adequacy of essential public electricity utilities. Furthermore, scanned road networks can assist residents in planning effective evacuation routes. Collectively, the segmentation enables planners to better understand the socio-economic dynamics and living conditions within favelas, thereby facilitating informed policies aimed at promoting economic development, social equity, and environmental sustainability.

Even with the inherent difficulties posed by unstructured LiDAR point cloud data, this research successfully developed and validated an AI-based framework for analyzing complex urban morphologies typical of informal settlements. This framework effectively captures and characterizes critical urban features, including the intricate 3D street networks, variations in building geometries, color attributes, and detailed internal structures. This research contributes to a practical and cost-effective framework for detecting and monitoring favelas, offering substantial improvements over traditional, manual methods. Moreover, this research is the first to apply the 3DMASC machine learning method specifically for automated semantic segmentation within favela environments. Therefore, the semantic segmentation procedure presented in this framework is scalable to other favelas or inaccessible areas, as its reproducible design allows the procedure to be readily transferred across contexts.

Collecting annual datasets using our framework would enhance our understanding of favela evolution, guiding urban planning and

policy interventions. Embracing the adaptability and resilience observed in favelas could inspire flexible urban planning approaches, fostering organic growth and community involvement rather than imposing rigid, top-down structures. In this way, cities can evolve as resilient, inclusive spaces that adapt to the diverse needs of their residents.

Another key practical implication of this research is the importance of community engagement and trust-building in data collection within informal settlements. Building mutual trust through transparent communication with community leaders, involving local residents in survey planning and execution, and respecting cultural sensitivities—such as appropriate color choices for survey markers and safeguarding residents' privacy—were essential for the successful execution of the LiDAR surveys. Such inclusive and respectful practices not only foster community cooperation but also enhance the validity and social acceptance of the collected data and the resulting analysis. Community engagement is also essential for evaluating the generalizability of the framework in other locations in future studies.

In conclusion, this research introduced a reproducible framework for 3D LiDAR semantic segmentation of favela morphologies, demonstrating its ability to capture complex urban features and advancing automated analysis beyond traditional manual methods. As the first application of the 3DMASC machine learning approach in this context, the study establishes a scalable tool for detecting and monitoring informal settlements.

This research has certain limitations that must be acknowledged along with corresponding suggestions for future research. Firstly, the dataset and analyses were limited to a relatively small sample of LiDAR point clouds from the Vidigal favela. Future research should validate these findings across diverse informal settlements. Secondly, while our current analysis focused on scale-level feature contributions using Sharply values, future research could build on this work by incorporating systematic ablation experiments. This can provide further validation of our findings and refine our understanding of the relative importance of specific feature groups in dense and complex settlement environments. Thirdly, the segmentation step in this research relied on the existing 3DMASC machine learning method. Developing a novel segmentation algorithm specifically tailored to the unique challenges posed by informal urban settings could further enhance segmentation accuracy and applicability. A potential limitation of 3DMASC is its sensitivity to rotation. Since several of the descriptors, such as height-based statistics and elevation skewness, are computed in fixed spatial coordinates, the resulting features are not strictly rotation invariant. While this does not strongly affect our case study, where acquisition followed relatively consistent orientations, it may reduce robustness under arbitrary orientations of wearable LiDAR scans. Future work could address this by incorporating rotation-invariant descriptors or data augmentation strategies. The class imbalance in the dataset, with buildings and ground dominating, likely explains the higher performance of these classes. Future work should address this imbalance through data augmentation, re-sampling, or incorporating additional training data. Moreover, favelas have other classes that can be segmented, such as windows and doors. Knowing the positions of windows and doors in each building can facilitate further subsequent analysis. For instance, 3D models with window and door locations built and segmented from collected point cloud datasets can be applied to airflow simulation to help settlements improve the airflow and decrease airborne disease transmission, which could be a future research direction.

Methodology

Framework of this research

This research applied machine learning to achieve the automated detection of favelas' information. Machine learning was chosen because it is a repeatedly validated and feasible approach. Some state-of-the-art deep learning models, such as PointNet++⁴², KPConv⁴³, and Point Transformer²¹ have shown impressive performance on large-scale datasets. However, their advantages over machine learning are not always guaranteed in certain urban scenarios. For instance, Rashdi et al.⁴⁴ systematically

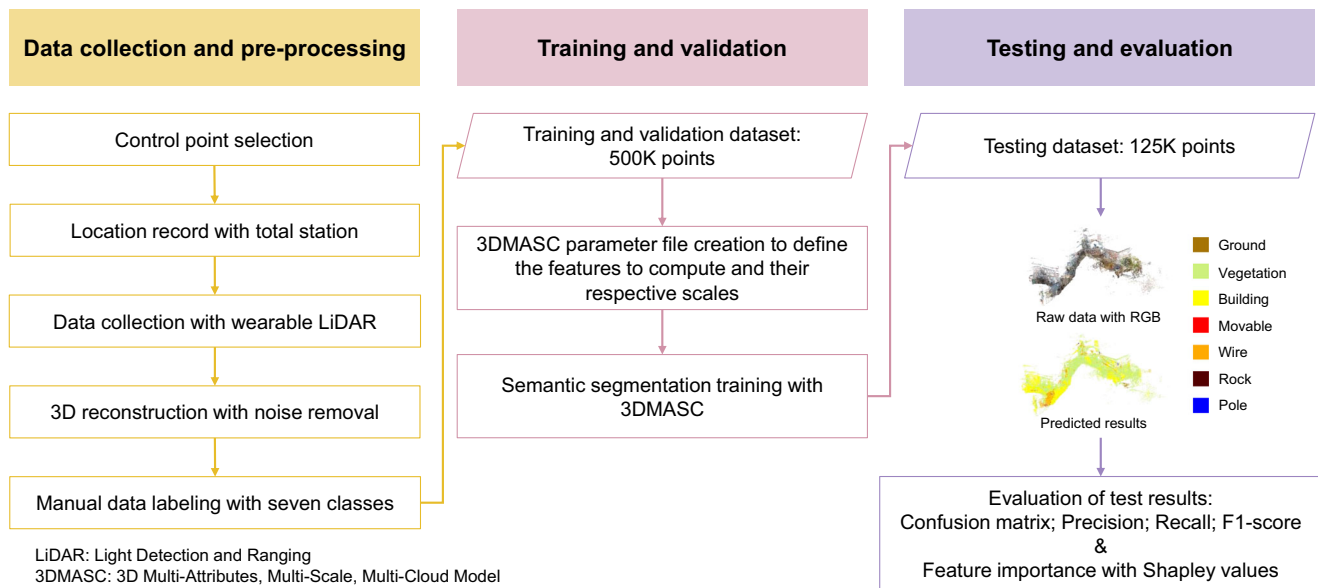


Fig. 7 | Framework of the research. This framework contains three main sections: data collection and pre-processing, training and validation, and testing and evaluation. LiDAR point clouds were scanned and pre-processed to prepare datasets for training and testing. Then, 3DMASC with pre-trained parameters was applied for

training and validation. After that, the trained model was applied to test the semantic segmentation results, including seven classes. Several metrics were applied to evaluate the performance of the model. The importance of the feature was also estimated using Shapley values.

compared random forest, support vector machine, and neural networks on mobile LiDAR data for segmentation of buildings and roads in cities, and random forest performed best. In land cover classification using colorized LiDAR data, random forest outperformed neural networks in terms of overall accuracy and the Kappa index for detecting building, vegetation, and road, which are three classes detected in this research⁴⁵. Taher et al.⁴⁶ showed that on sparse multispectral LiDAR data, random forest outperformed a Point Transformer, illustrating that traditional models can be more robust when points are sparser for tree segmentation, similar to vegetation sparsity in this research, caused by the difficulty of scanning tree tops. In addition, most existing state-of-the-art deep learning models were developed for wide, open roads and city-scale environments, whereas this research focuses on narrow alleyways and streets typical of informal settlements. Moreover, deep learning always demands extensive training data, which is not feasible to obtain in this research. Given these considerations, a random forest-based machine learning model proposed in 2024 with fewer training data requests, 3DMASC, was chosen, considering our limited data. The framework of this research is illustrated in Fig. 7.

Study area and data acquisition

The LiDAR data collection survey was conducted on December 12, 2024, in Vidigal, Brazil. As mentioned in the Introduction Section, large favelas in Rio are primarily located on hilly sites. As one of the biggest favelas in Rio, Vidigal is built on a mountain with several buildings and other facilities, so its environment is complex. It is in the southern coastal area of Rio, near Ipanema Beach, looking out over the Atlantic Ocean⁴⁷, which is shown in Fig. 8. Vidigal borders Gávea, Leblon, and São Conrado. Historically, these southern zones of Rio are those where middle and upper-income households reside³¹. Across the mountain, where Vidigal is, lies the largest favela in Rio, Rocinha. This means that wealthy families and impoverished populations live nearby, which is an exciting social phenomenon that needs to be studied. Therefore, this research chose Vidigal as the case study.

To conduct the survey in the favela, we previously agreed with local resident representatives on the path to be taken, and we obtained permission to enter Vidigal. This communication is essential to ensure transparency and foster collaboration throughout the process. All field surveys were

accompanied by a resident representative from the area. Throughout data collection and processing, we took care to avoid exposing personally identifiable features or sensitive household information. All point cloud data were anonymized, and the mapping effort was designed to minimize social risk and maximize community benefit.

Data collection involves selecting control points, setting up a total station for geo-coordinate measurement and recording, and collecting point cloud data using a wearable LiDAR device. Figure 9 is the in-situ photos taken during these three steps, shown from left to right. Control points are physically coordinated locations used to establish a consistent system for 2D mapping and 3D reconstruction, which are necessary for connecting scanned point clouds⁴⁸. These control points serve as georeferencing anchors, ensuring the accurate alignment of data throughout the mapped network. This research set control points using yellow paint, as labeled in Fig. 9. Our team first designed some planned points based on open-source high-resolution satellites. During the design of control points, it was found that some alleys are obscured by eaves in satellite images. Therefore, the setting of control points was carried out on two field trips. The first trip was to observe the environments of the planned scanned areas. The second trip was to paint several control points. Finally, we chose the locations with three control points, SV24, SV25, and SV26, to scan favela streets and alleys.

After painting the control points, to support the georeferencing of the LiDAR survey, a GNSS Topcon Hiper VR and a Leica TC407 Total Station were used to record the precise locations, elevations, and coordinates of the control points. Table 3 presents the main technical specifications and features of the total station. Battery specifications are noted, with a 5-h autonomy powered by NiMH batteries, ensuring sufficient operational duration. Communication is facilitated via an RS232 interface, and the internal memory can store up to 10,000 points. Additionally, the instrument is lightweight (5.2 kg) and designed with precision in mind, offering an angular accuracy of 7'' and a linear accuracy of 2 mm plus 2 ppm. Other features include a laser plummet for precise vertical alignment and an IP55 rating for dust and water resistance. Notably, the device offers a range of 3500 m, a telescope magnification of 30×, and a field of view of 1° 30'. After the location record with the total station, the survey was carried out using a



Fig. 8 | Scanned location and control points in Vidigal. Three control points were labeled as yellow before the LiDAR scanning, shown in the bottom right corner.

Fig. 9 | In-situ survey for LiDAR data collection. Data collection involves selecting and labeling control points using yellow paint, setting up a total station for geo-coordinate measurement and recording, and collecting point cloud data using a wearable LiDAR device.



wearable simultaneous localization and mapping (SLAM)-based LiDAR device. Table 4 outlines the features of the device utilized. This sensor system is engineered for high-resolution, rapid data acquisition in complex urban environments such as favelas. It boasts a maximum range of 50 m and an impressive scanning speed of 2×600 K points per second, which allows for the detailed mapping of densely populated, irregularly structured areas. Its local accuracy ensures that even small details in the physical environment are captured precisely. Equipped with four cameras offering a color resolution of 4×20 megapixels, the system delivers high-quality imagery. The 360° horizontal and vertical field of view provides comprehensive situational awareness, which is

critical for understanding the spatial configuration and potential vulnerabilities within informal settlements. The device is powered by two Li-ion batteries, offering 1.5 h of runtime, and despite its robust capabilities, it maintains a manageable weight of 8.68 kg (including batteries), making it suitable for deployment in the often challenging terrains of favelas.

After getting the scanned raw data, noises were removed from these raw points, and the 3D model from the point clouds was built with SLAM technology based on the control points and location records. After that, seven classes were manually labeled in CloudCompare for the machine learning model training and testing. The scanned data were then analyzed to

Table 3 | General description of the total station device

Specification and feature	Value
Range (with 1 prism)	3500 m
Telescope magnification	30×
Battery autonomy	5 hours
Battery type	NiMH
Field of view	1°30'
Compensator	Dual-axis
Communication interface	RS232
Internal memory	10,000 points
Circular level	6/2 mm
Weight	5.2 kg
Angular accuracy	7"
Linear accuracy	2 mm + 2 ppm
Laser plummet	Yes
Dust and water resistance	IP55
Display type	LCD (280 × 160 pixels)

Table 4 | General description of the LiDAR device

Specification and feature	Value
Maximum range	50 m
Scanning speed	2 × 600,000 pts/sec
Accuracy (according to Guides)	6 mm (local)
Color resolution	4 × 20 MPx
Camera	4 cameras
Field of view (FOV)	360° horizontal/360° vertical
Battery	2× Li-ion, 1.5 h runtime
Weight	8.68 kg (with batteries)
Resistance	IP42
Software	Not specified
Operating conditions	0 °C to 40 °C (operational), -10 °C to 40 °C (non-operational)

unveil the internal spatial morphology of favelas using machine learning techniques, which cannot be detected from observations using satellite or airborne imagery.

Morphology observation of collected point clouds

We scanned streets in the Vidigal favela, covering a total area of 2636 m², as shown in Fig. 10, which is the empty area in Google Maps and OpenStreetMap. Fig. 10a displays the collected point cloud data with color information, which has a resolution of 10 mm and contains 63,571,970 points, using the EPSG:31983 coordinate system. Figure 10b, c display top and side views of the scanned unstructured raw point cloud, which illustrate the survey quality report, including the scanning trajectory, locations where panoramic images were captured, and control points. These views collectively capture the intricate spatial arrangement and vertical layering that characterize this informal urban setting. The top view of the scanned area (Fig. 10b) highlights the spatial distribution and density of the point cloud. Networks of interconnected roads are captured through linear yellow trajectories, while SLAM keypoints are indicated by red reference markers. Surveyed places in the top-view map also reveal variations in road width, curvature, and branching intersections, which are common morphological features of favelas. Meanwhile, the side views (Fig. 10c) demonstrate the vertical complexity, including the irregular elevation profiles and sloped terrains of the Vidigal favela. It also highlights vertical structures within its scenes, such as utility or light poles, overhead wires, and tree canopies.

Overall, this comprehensive scan not only provides a detailed representation of distinct physical elements within the favela but also offers valuable insights into the environmental and social characteristics of these areas. For instance, ground features, including road width and surface conditions, reflect mobility and access challenges within the dense urban fabric, while building structures imply housing density and vertical expansion that shed light on spatial constraints and informal construction practices within favelas³¹. The presence and distribution of vegetation indicate green space availability and potential environmental resilience⁴⁹. Electrical wires and poles that support the cables are also captured by the collected point clouds, illustrating the state of public electricity facilities⁵⁰. Additionally, we consider rocks as an observation that indicates an important physical feature in steep hillside terrain^{51,52}. Therefore, we identify these features as necessary object categories to be classified using wearable LiDAR.

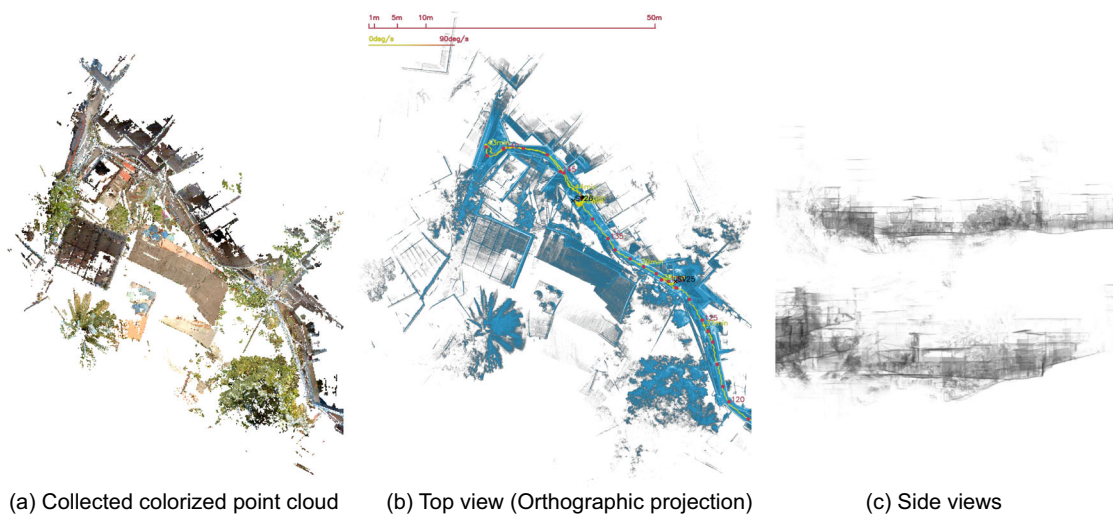


Fig. 10 | Information on scanned colored LiDAR point clouds. **a** Collected point cloud data with color information, which has a resolution of 10 mm and contains 63,571,970 points, using the EPSG:31983 coordinate system. **b** Top view of the scanned unstructured raw point cloud. Networks of interconnected roads are

captured through linear yellow trajectories, while simultaneous localization and mapping (SLAM) keypoints are indicated by red reference markers. **c** Side views of the scanned LiDAR data.

Examining these features can help us better understand the spatial organization and hint at the socio-environmental dynamics of favelas, guiding interventions to improve living conditions and infrastructure development.

Data availability

The datasets generated and analyzed during the current study are not publicly available because a stand-alone data paper describing the dataset is currently in preparation, but they are available from the corresponding author on reasonable request.

Received: 3 May 2025; Accepted: 28 October 2025;

Published online: 10 December 2025

References

- United Nations Department of Economic and Social Affairs. *The Sustainable Development Goals Report* (United Nations Department of Economic and Social Affairs, 2023).
- United Nations. *SDG Progress Report* (United Nations, 2024).
- Cervero, R., Guerra, E. & Al, S. The global south. *Beyond Mobility: Planning Cities For People and Places* (Island Press, 2017).
- Ngo, N. S. et al. Occupational exposure to roadway emissions and inside informal settlements in sub-Saharan Africa: a pilot study in Nairobi, Kenya. *Atmos. Environ.* **111**, 179–184 (2015).
- Corburn, J. & Sverdluk, A. Informal settlements and human health. *In Proc. Integrating Human Health Into Urban And Transport Planning: A Framework*, 155–171 (Springer, 2018).
- Abunywah, M., Gajendran, T. & Maund, K. Profiling informal settlements for disaster risks. *Procedia Eng.* **212**, 238–245 (2018).
- Camacho, R., Aryal, J. & Rajabifard, A. Disaster-induced disruption of policies for informal urban settlements. *Cities* **150**, 105098 (2024).
- Usamah, M., Handmer, J., Mitchell, D. & Ahmed, I. Can the vulnerable be resilient? Co-existence of vulnerability and disaster resilience: informal settlements in the Philippines. *Int. J. Disaster Risk Reduct.* **10**, 178–189 (2014).
- Ono, H. & Adrien, U. Community-driven informal settlement upgrading as an everyday practice: the role of urban and governance policies. *Land Use Policy* **146**, 107318 (2024).
- Rehman, M. F. U., Aftab, I., Sultani, W. & Ali, M. Mapping temporary slums from satellite imagery using a semi-supervised approach. *IEEE Geosci. Remote Sens. Lett.* **19**, 1–5 (2022).
- Raj, A., Mitra, A. & Sinha, M. Deep learning for slum mapping in remote sensing images: a meta-analysis and review. *arXiv preprint* <https://doi.org/10.48550/arXiv.2406.08031> (2024).
- Stark, T., Wurm, M., Zhu, X. X. & Taubenböck, H. Quantifying uncertainty in slum detection: advancing transfer learning with limited data in noisy urban environments. *IEEE J. Sel. Top. Appl. Earth Observ. Remote Sens.* **17**, 4552–4565 (2024).
- Ribeiro, S., Jarzabek-Rychard, M., Cintra, J. & Maas, H.-G. Describing the vertical structure of informal settlements on the basis of lidar data—a case study for favelas (slums) in São Paulo City. *ISPRS Ann. Photogramm. Remote Sens. Spat. Inf. Sci.* **4**, 437–444 (2019).
- Gevaert, C., Persello, C., Sliuzas, R. & Vosselman, G. Informal settlement classification using point-cloud and image-based features from UAV data. *ISPRS J. Photogramm. Remote Sens.* **125**, 225–236 (2017).
- Hofmann, P., Taubenböck, H. & Werthmann, C. Monitoring and modelling of informal settlements—a review on recent developments and challenges. *Jt. Urban Remote Sens. Event* **2015**, 1–4 (2015).
- Griffith-Charles, C. & Sutherland, M. 3D cadastres for densely occupied informal situations: necessity and possibility. *Land Use Policy* **98**, 104372 (2020).
- Qi, C. R., Su, H., Mo, K. & Guibas, L. J. Pointnet: deep learning on point sets for 3d classification and segmentation. *Proc. IEEE Conf. Comput. Vis. pattern Recognit.* **1**, 652–660 (2017).
- Zhou, Y. & Tuzel, O. Voxelnet: End-to-end learning for point cloud based 3d object detection. In *Proc. IEEE Conference On Computer Vision and Pattern Recognition*. 4490–4499 (IEEE, 2018).
- Wang, Y. et al. Dynamic graph cnn for learning on point clouds. *ACM Trans. Graph* **38**, 1–12 (2019).
- Hu, Q. et al. Learning semantic segmentation of large-scale point clouds with random sampling. *IEEE Trans. Pattern Anal. Mach. Intell.* **44**, 8338–8354 (2021).
- Zhao, H., Jiang, L., Jia, J., Torr, P. H. & Koltun, V. “Point transformer,”. In *Proc. IEEE/CVF International Conference On Computer Vision*, 16259–16268 (IEEE, 2021).
- Miao, Y., Sun, Y., Zhang, Y., Wang, J. & Zhang, X. An efficient point cloud semantic segmentation network with multiscale super-patch transformer. *Sci. Rep.* **14**, 14581 (2024).
- Behley, J. et al. Semantickitti: a dataset for semantic scene understanding of lidar sequences. In *Proc. IEEE/CVF International Conference on Computer Vision*. 9297–9307 (IEEE, 2019).
- Roynard, X., Deschaud, J.-E. & Goulette, F. Paris-Lille-3D: A large and high-quality ground-truth urban point cloud dataset for automatic segmentation and classification. *Int. J. Robot. Res.* **37**, 545–557 (2018).
- Tan, W. et al. Toronto-3d: a large-scale mobile lidar dataset for semantic segmentation of urban roadways. In *Proc. IEEE/CVF Conference on Computer Vision and Pattern Recognition Workshops*. 202–203 (IEEE, 2020).
- Li, X. et al. Campus3d: a photogrammetry point cloud benchmark for hierarchical understanding of outdoor scene. In *Proc. 28th ACM International Conference on Multimedia*. 238–246 (ACM, 2020).
- Wysocki, O. et al. Zaha: Introducing the level of facade generalization and the large-scale point cloud facade semantic segmentation benchmark dataset. In *Proc. IEEE/CVF Winter Conference on Applications of Computer Vision (WACV)*. 7648–7658 (IEEE, 2025).
- Edelman, D. J. Managing the urban environment of Rio de Janeiro, Brazil. *Curr. Urban Stud.* **12**, 123–151 (2024).
- Perlman, J. E. The myth of marginality revisited: the case of favelas in Rio de Janeiro. *Becoming global and the new poverty of cities*. <https://www.urbanleaders.org/540UrbanReality/14Marginality/perlman.pdf> (2005).
- Rio City Government. *Definition of Favelas*, <https://sabren-pcrj.hub.arcgis.com/pages/favelas> (2024).
- Salazar Miranda, A. et al. Favelas 4D: scalable methods for morphology analysis of informal settlements using terrestrial laser scanning data. *Environ. Plan. B Urban Anal. City Sci.* **49**, 2345–2362 (2022).
- Lauterbach, H. A. et al. Evaluation of a backpack-mounted 3D mobile scanning system. *Remote Sens.* **7**, 13753–13781 (2015).
- Zhang, W. et al. An easy-to-use airborne LiDAR data filtering method based on cloth simulation. *Remote Sens.* **8**, 501 (2016).
- Letard, M. et al. 3DMASC: accessible, explainable 3D point clouds classification. Application to Bi-spectral Topo-bathymetric lidar data. *ISPRS J. Photogramm. Remote Sens.* **207**, 175–197 (2024).
- Esri. *What is Lidar Intensity Data?*, <https://desktop.arcgis.com/en/arcmap/latest/manage-data/las-dataset/what-is-intensity-data.htm> (2024).
- Brodu, N. & Lague, D. 3D terrestrial lidar data classification of complex natural scenes using a multi-scale dimensionality criterion: applications in geomorphology. *ISPRS J. Photogramm. Remote Sens.* **68**, 121–134 (2012).
- Weinmann, M., Jutzi, B. & Mallet, C. Feature relevance assessment for the semantic interpretation of 3D point cloud data. *ISPRS Ann. Photogramm. Remote Sens. Spat. Inf. Sci.* **2**, 313–318 (2013).
- Shapley, L. S. A value for n-person games. *Contributions to Theory Games* 307–317 (Princeton University Press, 1953).

39. Zhu, Q., Cao, J., Cai, Y. & Fan, L. Evaluating the impact of point cloud colorization on semantic segmentation accuracy. In *Proc. IEEE 8th International Conference on Vision, Image and Signal Processing (ICVISP)* 1–5 (IEEE, 2024).
40. El Madawi, K. et al. RGB and LiDAR fusion based 3d semantic segmentation for autonomous driving. In *Proc. IEEE Intelligent Transportation Systems Conference (ITSC)*. 7–12 (IEEE, 2019).
41. Aijazi, A. K., Checchin, P. & Trassoudaine, L. Segmentation based classification of 3D urban point clouds: a super-voxel based approach with evaluation. *Remote Sens.* **5**, 1624–1650 (2013).
42. Qi, C. R., Yi, L., Su, H. & Guibas, L. J. Pointnet++: Deep hierarchical feature learning on point sets in a metric space. In *Proc. 31st International Conference on Neural Information Processing Systems* **30** (Curran Associates Inc., 2017).
43. Thomas, H. et al. Kpconv: flexible and deformable convolution for point clouds. In *Proc. IEEE/CVF International Conference on Computer Vision*. 6411–6420 (IEEE, 2019).
44. Rashdi, R., Balado, J., Sánchez, J. & Arias, P. Comparative study of road and urban object classification based on mobile laser scanners. *Int. Arch. Photogramm. Remote Sens. Spat. Inf. Sci.* **48**, 423–429 (2023).
45. Taha, L. G. E.-D. & Mandouh, A. A. Assessment of random forest and neural network for improving land use/land cover mapping from LIDAR data and rgb image: a case study of magaga-EI-menia governorate, egypt. *Geoplanning J. Geomat. Plan.* **11**, 17–30 (2024).
46. Taher, J. et al. Multispectral airborne laser scanning for tree species classification: a benchmark of machine learning and deep learning algorithms. *arXiv preprint* <https://doi.org/10.48550/arXiv.2504.14337> (2025).
47. Törnberg, P. & Uitermark, J. Urban mediatization and planetary gentrification: The rise and fall of a favela across media platforms. *City Commun.* **21**, 340–361 (2022).
48. Schofield, W. & Breach, M. *Engineering Surveying* (CRC Press, 2007).
49. Münzinger, M., Prechtel, N. & Behnisch, M. Mapping the urban forest in detail: from LiDAR point clouds to 3D tree models. *Urban Forestry Urban Green.* **74**, 127637 (2022).
50. Inoue, M. et al. Visualization of 3D cable between utility poles obtained from laser scanning point clouds: a case study. *SN Appl. Sci.* **3**, 860 (2021).
51. Blanco, L. et al. Machine learning-based rockfalls detection with 3d point clouds, example in the Montserrat massif (Spain). *Remote Sens.* **14**, 4306 (2022).
52. Weidner, L., Walton, G. & Kromer, R. Classification methods for point clouds in rock slope monitoring: a novel machine learning approach and comparative analysis. *Eng. Geol.* **263**, 105326 (2019).
53. Hackel, T., Wegner, J. D. & Schindler, K. Fast semantic segmentation of 3D point clouds with strongly varying density. *ISPRS Ann. Photogramm. Remote Sens. Spat. Inf. Sci.* **3**, 177–184 (2016).

Acknowledgements

The authors acknowledge Sondotécnica for providing both technical equipment and field professionals, including Boaz Teixeira, who operated the LiDAR equipment, and Júlia Araujo Mantovani Silotto, who coordinated the fieldwork. The authors also acknowledge Rural Tech, which provided the LiDAR equipment, and Serra Verde for the topographic team.

Author contributions

C.L. and F.D. defined the problem. C.L., K.J., and C.B. designed the research. S.D. and C.B. collected data. C.L., K.J., S.D., and C.B. performed the analysis, supervised by F.D. and C.R. C.L. and K.J. wrote the original manuscript. C.L., K.J., and F.D. revised the manuscript. All authors participated in the discussion and reviewed the manuscript.

Competing interests

The authors declare no competing interests.

Additional information

Correspondence and requests for materials should be addressed to Fabio Duarte.

Reprints and permissions information is available at

<http://www.nature.com/reprints>

Publisher's note Springer Nature remains neutral with regard to jurisdictional claims in published maps and institutional affiliations.

Open Access This article is licensed under a Creative Commons Attribution-NonCommercial-NoDerivatives 4.0 International License, which permits any non-commercial use, sharing, distribution and reproduction in any medium or format, as long as you give appropriate credit to the original author(s) and the source, provide a link to the Creative Commons licence, and indicate if you modified the licensed material. You do not have permission under this licence to share adapted material derived from this article or parts of it. The images or other third party material in this article are included in the article's Creative Commons licence, unless indicated otherwise in a credit line to the material. If material is not included in the article's Creative Commons licence and your intended use is not permitted by statutory regulation or exceeds the permitted use, you will need to obtain permission directly from the copyright holder. To view a copy of this licence, visit <http://creativecommons.org/licenses/by-nc-nd/4.0/>.

© The Author(s) 2025